The Morphology of Macroscopic Soot

C. M. Sorensen and G. D. Feke†*
DEPARTMENT OF PHYSICS, KANSAS STATE UNIVERSITY, MANHATTAN, KS 66506-2601

ABSTRACT. The morphology of soot collected from a laminar acetylene/air diffusion flame was studied. Collection methods included both thermophoretic and impaction sampling from both the luminous and nonluminous portions of the flow. The soot was viewed with both electron and optical microscopy. Cluster sizes ranged over four orders of magnitude from 50 nm to 400 μm to include some clusters visible to the naked eye. A new method of micrograph analysis, necessary when the clusters were large, was developed to account for the unresolved primary particles. Over this entire size range, the same fractal morphology was found with a fractal dimension of $D = 1.8$ and, within a rather large uncertainty, the same prefactor $k_0 = 1.7$. Thus, the fractal morphology of soot remains constant from clusters of about 10 primary particles per aggregate to macroscopic clusters of over 10^8 primary particles. AEROSOL SCIENCE AND TECHNOLOGY 25:328–337 (1996).

INTRODUCTION

Considerable effort has been made to study the morphology of soot aggregates that are produced by hydrocarbon flames (Medalia and Heckman, 1967, 1969; Forrest and Witten, 1979; Samson et al., 1987; Bourrat et al., 1988; Zhang et al., 1988; Megaridis and Dobbins, 1990; Gangopadhyay et al., 1991; Charalampopoulos and Chang, 1991; Sorensen et al., 1992a, 1992b; Puri et al., 1993; Cai et al., 1993, 1995; Koylu et al., 1992, 1994a, 1994b, 1995). Consequently, it is now well established that these aggregates are composed of small, on the order of a few tens of nanometers, primary particles which are randomly clustered together. These primary particles, or monomers, are roughly spherical and mostly carbon in content. The nondense clusters have a fractal morphology so that the number of primary particles per aggregate N scales with the overall size of the aggregate, which may be quantified by the cluster radius of gyration R_g, with a power D less than the spatial dimension of three as described by

$$N = k_0 (R_g/a)^D. \quad (1)$$

In Eq. (1), a is the primary particle radius, D is the fractal dimension, and k_0 is the prefactor of the scaling relationship. A summary of past work is given in Table 1 where it is seen that the fractal dimension of the soot has typically been found to be equal to ~ 1.75. The ability to describe the soot aggregate morphology is important in a number of applications, including understanding the soot optics, radiative transfer, and kinetics of growth.

Often, soot is emitted from a flame, and under certain circumstances, the individual clusters are large enough to be visible to the naked eye. Examples include soot from

*To whom correspondence should be addressed.
†Current address: Department of Mechanical Engineering, Yale University, New Haven, CT 06520.

0278-6826/96/$15.00
PII S0278-6826(96)00078-5

Aerosol Science and Technology 25:328–337 (1996)

Published by Elsevier Science Inc.

TABLE 1. Soot Morphological Measurements

Investigators	Soot Source	Method	D	k_0	Max Size
Medalia & Heckman (1967, 1969)	Carbon Black	TEM	—	—	
Sampson et al. (1987)	C_2H_2 Diff. post flame	TEM	1.5–1.8	—	13 μm
Megaridis & Dobbins (1987)	C_2H_4 Diff.	TEM	1.6–1.8	—	0.3 μm
Bourrat et al. (1988)	Carbon Black	TEM	1.46–1.80	—	< 1 μm
Zhang et al. (1988)	CH_4/O_2 premixed	TEM LS	1.72 ± 0.10 1.61 ± 0.06	—	~ 1 μm
Gangopadhyay et al. (1991)	CH_4/O_2 premixed	LS	1.6–1.8	—	0.2 μm
Charalampopoulos & Chang (1991)	C_3H_8/O_2 premixed	LS	1.74 ± 0.08	—	0.2 μm
Sorensen et al. (1992a, b)	CH_4/O_2 premixed	LS	1.70–1.79	—	0.2 μm
Koylu & Faeth (1992)	Many fuels large scale	TEM	1.70–1.79	—	3 μm
Puri et al. (1993)	C_2H_4 Diff.	LS TEM	1.74 ± 0.1	(2.4)	0.15 μm
Cai et al. (1993)	CH_4/O_2 premixed	TEM	1.70	—	0.2 μm
Koylu & Faeth (1994a, b)	Many fuels large scale	LS TEM	1.75–1.85	1.98–2.5	1 μm
Cai et al. (1995)	CH_4/O_2 premixed	TEM	1.74	1.23	0.15 μm
Koylu et al. (1995)	C_2H_2, C_2H_4, C_3H_6 C_3H_8 Diff.	TEM	1.65	2.71	0.5 μm
This work	C_2H_2 Diff.	TEM, OPT	1.8	1.7	400 μm

acetylene/air diffusion flames, polystyrene flames, and diesel emissions. All of the previous studies summarized in Table 1 studied much smaller soot, typically submicron with the largest on the order of 10 μm. In the context of these studies, it is relevant to ask what the morphology of such large clusters is and how it is the same or different from its smaller precursors. This is both of intrinsic interest since morphology is determined by the formation process and is at the foundation of understanding other physical properties, and practical value since this soot is released into the environment.

The purpose of this paper is to present a morphological study of soot obtained from both the luminous and nonluminous portions of a laminar acetylene flame in ambient air. The soot was examined by both electron and optical microscopy, and ranged in size from aggregates of a few primary particles with 23 nm radius up to nearly millimeter size aggregates, which is a four order of magnitude range. We find that all of this soot can be described as fractal with, remarkably, given the size range, the same fractal dimension of $D = 1.8$, and the same prefactor $k_0 \simeq 1.7$. In addition, analysis of very large soot clusters for which the primary particles were not resolved required a significant correction which has not been previously described, and hence our analysis will be useful to future studies of very large soot.

EXPERIMENTAL METHODS AND RESULTS

The Flame

A simple diffusion burner was made from a 0.9 cm i.d. brass tube with a screen cap to eliminate flashback. Acetylene passed through this tube at a flow rate of 3.2 cm^3/s, hence an average flow velocity of 5.0 cm/s at room temperature. The diffusion flame above this tube burned in ambient air. The flame was a bright yellow–white near its base, dulled to an orange by a height of about 5 cm above the burner lip

Aerosol Science and Technology
25:3 October 1996

and, thereafter darkened further to a black, laminar flow by 8 cm. This laminar flow continued to approximately 15 cm where it broke into turbulence.

Soot Sampling

Soot was collected by two different methods: thermophoretic and impaction sampling. During the initial period of this work, thermophoretic sampling was used. Average cluster sizes found on these samples were 0.3 μm or less for all heights above burner. Visual observation of the flame at large height showed a graininess which suggested that larger clusters might be present. Thus, impaction was used with the hope that this method's bias for larger sizes would capture any large clusters that might exist; and, in fact, clusters larger by $2\frac{1}{2}$ orders of magnitude were found. We believe that these large clusters truly exist in the aerosol and are not artifacts of the impaction collection technique. We base this on the fact that the cluster density on the surface of the impaction sampler was low; thus, the chance for overlap of clusters to make a large cluster is low. In fact, the cluster density for both the impaction and thermophoretic sampling was essentially the same so any overlap problem, or lack of it, would be the same in each method. Furthermore, we expect for both methods that the clusters hit and stick on the probe; they do not move around on the surface, and continue to find each other and aggregate. Finally, we remark that since it is our purpose to study large soot and not to characterize the flame, a sampling bias is of no consequence.

Thermophoretic Sampling on TEM Grids. Copper electron microscope grids with Formvar coating were placed on a "frog-tongue" probe device (Cai et al., 1993) designed after Dobbins and Megaridis (1987). This device injects the grids into the flame for a residence time of 15 ms; the time required for the grid to traverse the flame on entrance and exit was ~ 3 ms. Grids were held with their face in the vertical plane (parallel to the flame gas flow) and injected at eight different heights above the burner from 1.7 to 25.4 cm. TEM micrographs of the grids were photographically enlarged to a net magnification of $20800\times$. Figure 1a shows an example. The low surface density of clusters indicates that cluster overlap is not a problem. These photographs were scanned, and the digital representation of individual clusters was stored in a personal computer in a 16-level gray scale. The pictures were edited on the computer by visual comparison of the computer image to the photograph in order to remove all unwanted darkness in the picture background. This image was then converted to a binary format, with the ultimate result that the background was represented as white and the clusters represented as black. Calibration of the pixel elements of the digitized pictures to real sizes was performed to find the conversion factor $p = 12.1$ nm/pixel side. Programs were written to calculate projectional area and radius of gyration (see below).

The average monomer radius was determined by visual measurement of individual monomers and monomers in clusters with a $10\times$ magnifier equipped with a reticle. Only the thermophoretically sampled, TEM viewed clusters were used in this analysis because the impaction sampled, optical microscope viewed clusters did not have resolved monomers. The monomer radius was measured at all heights above the burner studied. The average monomer radius at a given height ranged from $a = 21$–28 nm with a very slight height dependency which indicated a maximum monomer radius near a height of 6 cm. However, the combined uncertainty and statistical fluctuation in a was ± 3 nm. Thus, this dependency is nearly within the uncertainty. This little or no height dependency is not surprising given the short extent of our luminous flame (~ 7 cm) and the large extent of our sampling (up to 25.4 cm). Most of the sampling was obtained from the post flame regime where the chemistry (surface growth or oxidation) is essentially done and physics (aggrega-

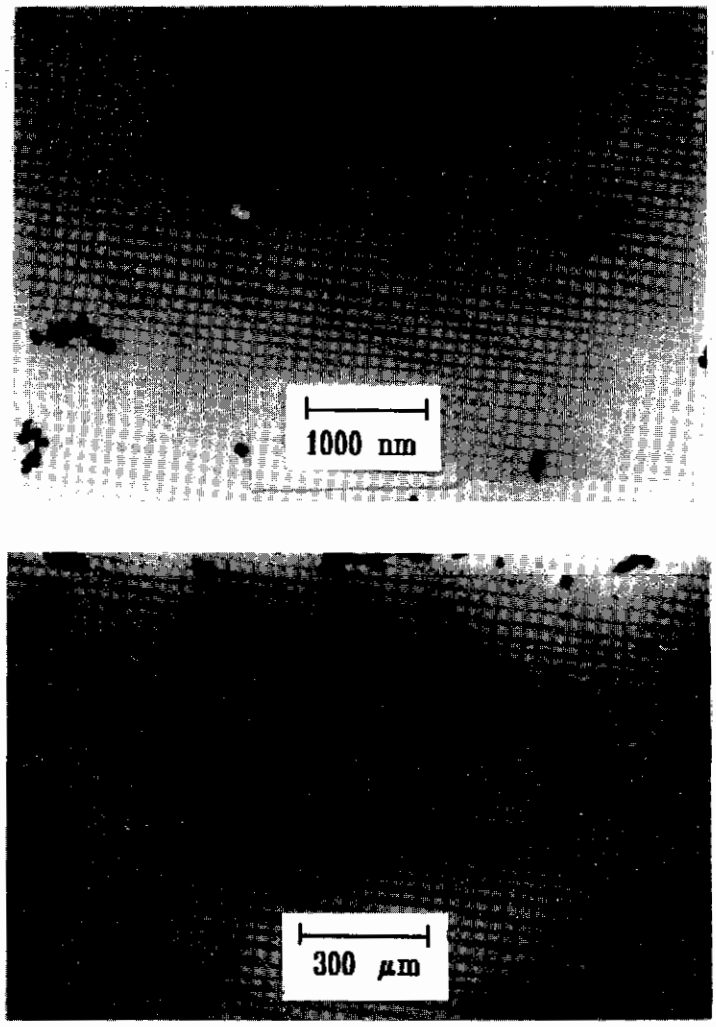

FIGURE 1. (a) TEM micrograph of soot collected by thermophoresis from the C_2H_2 in air diffusion flames. (b) Optical micrograph of soot collected by impaction. Note that despite the $2\frac{1}{2}$ order of magnitude difference between these two scales, the cluster morphology appears the same.

tion) is the cluster growth mechanism. Because of this, we will use a monomer radius average over all heights of $a = 23 \pm 3$ nm.

Impaction Sampling on Optical Microscope Slides. The sampling device was used again, but with standard glass microscope slides (25×75 mm) held with their plane perpendicular to the flow of the flame (i.e., horizontally). Thus, impaction was the major collection scheme. Residence times were again 15 ms. Insertion of the slide face perpendicular to the flow no doubt perturbs the flow, but since our goal is to determine the morphology of macroscopic soot clusters, this perturbation is not a deterrence. Samples were taken between 3.8 and 17.8 cm above the burner.

Aerosol Science and Technology
25:3 October 1996

Soot collected in this manner was significantly larger than soot collected via thermophoresis. In fact, some of the clusters were visible to the naked eye. Therefore, an optical microscope was used to take photographs of the impaction clusters. Obviously, the ~ 23 nm primary particles were not resolved. The net magnification to the photographic print was $72\times$. Figure 1b shows an example. These pictures were also scanned into a digital format and visually edited for computer analysis. The conversion factor was $p = 3.5$ μm/pixel side.

Analysis of Projected Images

A major problem in the analysis of the morphology of soot clusters lies in the fact that the three-dimensional structures are viewed as two-dimensional projections as a consequence of the microphotography. One way to overcome this is to view the clusters in at least two different projections, and with this stereo technique, regenerate the true three-dimensional structure. This has been done in the past (Samson et al., 1987; Koylu et al., 1995), but is untenable for our large soot clusters which have, as we shall see, as many as 10^8 primary particles, and for which the primary particles are not resolved. If, then, the analysis is limited to one projection, and if the density of this projection can give accurate information regarding the total mass along a given projection through the cluster, then a viable analysis of the three-dimensional morphology can be obtained. Such a mass preserving image is difficult to achieve, however, because the attenuation of the electrons or light which record the projected image is not linearly related to the total mass of soot through which it passed. Furthermore, the response of the photographic film that captures the image in either case is linear only over a small range before it saturates and becomes insensitive to the mass of the cluster above it. This leaves projection of the soot cluster onto the two-dimensional plane into a binary format, a shadow, in which any part of the cluster is the same degree of black as any other, and the background is white. The advantage of this method is that it eliminates the response of the detector, and it is straightforward. What is needed is a quantitative method to convert two-dimensional information into three-dimensional information, and we present such a method below.

Determination of N. Determination of N from the projected area of soot clusters has a long and well-established history (Medalia and Heckman, 1967, 1969; Samson et al., 1987; Megaridis and Dobbins, 1990; Koylu and Faeth, 1992; Cai et al., 1993, 1995; Koylu et al., 1992, 1994a, 1994b, 1995). In general it is found that

$$N = k_a(A_c/A_p)^{\alpha} \tag{2}$$

where k_a and α are constants near unity, and A_c and A_p are the projected areas of the cluster and primary particle, respectively. Medalia and Heckmann (1967, 1969) first used this form, and found empirically $k_a = 1.0$ and $\alpha = 1.1$. This has subsequently been corroborated by a number of workers with α varying by a few hundredths. Recently, Koylu et al. (1995) analyzed both computer-simulated and real soot clusters, and found $k_a = 1.15$–1.16 and $\alpha = 1.09$–1.10. A minor problem with these results is that the limit as $N \to 1$ is not preserved because k_a is not unity. In another simulation, Meakin et al. (1989) created DLCA clusters with $D = 1.8$ and N up to $N = 10^4$, larger than any in any other work that has compared N to the projected area. They fit their data with

$$A_c/A_p = 0.4784N + 0.5218N^{0.7689}. \tag{3}$$

This result is equivalent to Eq. (2) with $k_a = 1.00$ and $\alpha = 1.10$ over the range of $N = 1$–100 and $k_a = 1.00$ and $\alpha = 1.084$ over the range $N = 1$–1000. The slope of a log N versus $\log(A_c/A_p)$ graph is α, and Eq. (3) yields a slowly decreasing α with increasing N. This is consistent with the notion that, for clusters with $D < 2$, as $N \to \infty$, N should be linear with A_c, i.e., α asymptotically approaches 1.00, because the

cluster dimension is less than the dimension of the plane onto which it is projected.

Because of these comparisons, and since in our analysis of the TEM clusters the range of the number of primary particles is $10 < N < 2000$, we will use $k_a = 1.00$ and $\alpha = 1.09$. This is consistent with Eq. (3) and past work. For the optical clusters, the choice is not immediately evident because then, as will be shown below, $10^5 < N < 10^8$, and there is no precedent for Eq. (2) in this regime. One option is to use the asymptotic expectation $k_a = 1.00$ and $\alpha = 1.00$, but this ignores occultation near the center of the cluster. Because of our uncertainty, two forms will be used. We will use Eq. (2) with $k_a = 1.00$ and $\alpha = 1.09$. This has the advantage of being the same as that used for the TEM clusters. Given the trend in Eq. (3), however, at large N, this will be considered as an upper bound estimate on N. We will also use Eq. (3) directly, which represents an extrapolation by a factor of two in ln N space, i.e., to ln $N = 18$, beyond the data used to generate Eq. (3). Extrapolation can be dangerous, but Eq. (3) appears well behaved in that the overall slope it yields between ln $N = 0$ and ln $N = 18$ is $\alpha = 1.042$.

Determination of R_g. The radius of gyration R_g of a three-dimensional body is given by

$$R_g^2 = \int r^2 \rho(r) d^3r / \int \rho(r) d^3r \qquad (4)$$

where $\rho(r)$ is the assumed spherically symmetric density. Fractal clusters are not spherically symmetric, but for our analysis, we shall make the reasonable assumption that an ensemble of clusters on a TEM grid or microscope slide when viewed from one direction will yield an average spherical symmetry. Then, since $r^2 = x^2 + y^2 + z^2$, and since a projection onto a plane eliminates one of the dimensions, it follows from Eq. (4) that

$$R_{g,3} = \sqrt{3/2}\, R_{g,\text{proj}}. \qquad (5)$$

In (5), $R_{g,3}$ is the true, three-dimensional radius of gyration of the cluster and $R_{g,\text{proj}}$ is that observed for the projected image. The factor 3/2 results from the elimination of one of the three dimensions. Furthermore, Eq. (5) applies to a mass preserving projection. Equation (5) is verified by the computer simulations of Koylu et al. (1995), who found the empirical factor relating the two radii to be 1.24 ± 0.01, in good agreement with $\sqrt{3/2} = 1.225$.

We have already discussed the difficulty in achieving a mass preserving projection, so we will use a two-dimensional binary representation of the soot cluster. It is well established that the fractal dimension of soot clusters is less than 2; typically, D is in the range 1.7–1.8. Thus, it might be expected that the projected image of a cluster onto a plane into a binary format would be mass conserving, i.e., no significant screening or occultation between monomers would occur. It should be stressed that this expectation is for asymptotically large clusters. For finite size clusters, screening occurs as demonstrated by Eq. (2) and the empirical fact that $\alpha > 1.0$. Thus, the effective fractal dimension in the two-dimensional plane of the binary projection should be different from the fractal dimension of the real, three-dimensional cluster. In the immediately following argument, we will call these fractal dimensions D_2 and D_3, respectively.

Consider how the three-dimensional cluster is projected onto the two-dimensional plane. With spherical or circular symmetry, we assume that the density profile of either the three-dimensional fractal cluster or its projection is given by

$$\rho(r) \propto r^{D-d}, \qquad \text{for } r \le R \qquad (6a)$$

$$= 0, \qquad \text{for } r > R \qquad (6b)$$

where R is the perimeter radius and $D = D_2$ or D_3, depending on the spatial dimension of $d = 2$ or 3 for the projected or real cluster, respectively. Then, Eq. (4) yields

$$R_{g,3}^2 = \frac{D_3}{D_3 + 2} R^2 \qquad (7)$$

and

$$R_{g,\text{binary}}^2 = \frac{D_2}{D_2 + 2} R^2. \qquad (8)$$

Thus, a relation between the true radius of gyration $R_{g,3}$ and the measured, binary projection radius of gyration $R_{g,\text{binary}}$ can be determined if we have a relation between D_3 and D_2.

To determine this latter relation, consider the empirical fact of Eq. (2) that $N_3 \sim A^{\alpha}$, where we now label the number of monomers with a subscript of three to designate that this is the number in three-dimensional space. We also have by Eq. (1), $N_3 \sim R_{g,3}^{D_3}$. The binary projection has analogous relations such that $N_2 \sim R_{g,\text{binary}}^{D_2}$ which defines D_2, but, and here is the key, $N_2 \sim A$. Furthermore, by Eqs. (7) and (8), $R_{g,3} \sim R_{g,\text{binary}}$. All of these proportionalities together yield

$$D_2 = D_3/\alpha. \tag{9}$$

This result is consistent with past work that has measured the fractal dimension of clusters both in terms of three-dimensional quantities and projectional quantities to find that the projectional dimension is typically 10% less than that determined with the three-dimensional quantities (Samson et al., 1987; Zhang et al., 1988; Cai et al., 1993). It is also consistent with recent simulations by Jullien et al. (1994), who also found the projectional fractal dimension to be $\sim 10\%$ less than the fractal dimension of the unprojected clusters. Since $\alpha \simeq 1.1$, we believe that Eq. (9) explains these past observations.

Finally, we use Eqs. (7)–(9) to find

$$R_{g,3} = \left(\frac{D_3 + 2\alpha}{D_3 + 2}\right)^{1/2} R_{g,\text{binary}}. \tag{10}$$

For typical values of $D_3 = 1.8$ and $\alpha = 1.09$, this correction factor is 1.023. Thus, as anticipated and qualitatively explained earlier (Cai et al., 1993), the binary projection yields a remarkably accurate measure of the true, three-dimensional radius of gyration.

Computer Analysis. To begin our computer analysis of the clusters, we define the total darkness as

$$D_{\text{tot}} = \sum_{x,y} D(x,y) \tag{11}$$

where $D(x,y) = 0$ or 1 is the darkness of the pixel at position (x,y). Since $D(x,y)$ is binary, D_{tot} is the total number of pixels in a cluster n. The cluster projectional area is given by $A_c = np^2$.

To determine the radius of gyration R_g of a cluster, we first calculate the cluster center of mass:

$$\vec{r}_{cm} = D_{\text{tot}}^{-1} \sum_{x,y} D(x,y)\vec{r}(x,y) \tag{12}$$

and then the radius of gyration:

$$R_{g,\text{binary}}^2 = D_{\text{tot}}^{-1} \sum_{x,y} D(x,y)\left(\vec{r}(x,y) - \vec{r}_{cm}\right)^2. \tag{13}$$

Between 30 and 100 clusters were analyzed to obtain N and R_g for each of the eight heights above the burner where soot was collected for both the TEM and optical samples.

These data sets were then analyzed in accordance with Eq. (1). We found that individual heights above the burner yielded consistent values of D and k_0, and the D values were the same between the TEM and optical samples, but the k_0 values were different. Because of this, we have grouped together all of the data at different heights for the TEM and optical samples individually, and analyzed these two ensembles with Eq. (1). A total of 824 clusters were analyzed. The results are given in Table 2. Table 2 shows fractal dimensions of $1.84 \pm$

TABLE 2.

Sample	D	k_0 (uncorrected)	k_0 (corrected)
TEM	1.84 ± 0.11	1.66 ± 0.4	—
Optical ($\alpha = 1.09$)	1.78 ± 0.05	19.8 ± 7	2.0 ± 0.9
Optical ($\alpha = 1.042$)	1.70 ± 0.05	17.8 ± 6	2.0 ± 0.9

0.11 for the TEM sample and 1.78 ± 0.05 and 1.70 ± 0.05 for the optical sample analyzed in the two different ways. All of these values are both consistent with each other and previous work (Table 1). The k_0 values, however, are drastically different. For the TEM sample, $k_0 = 1.66 \pm 0.35$, which is comparable but larger than previous work in our lab for soot collected from premixed CH_4/O_2 flames where we found $k_0 = 1.23 \pm 0.07$ (Cai et al., 1995). It is also similarly larger than values inferred by Wu and Friedlander (1993) from a review of computer simulations who found $k_0 =$ 1.0–1.5. It is lower than the values found by Koylu et al. (1994a, 1994b, 1995) of ~ 2.4. We do not, at this time, understand the reason for these discrepancies. In contrast are the very large values of k_0 for the optical soot. What is the source of this latter discrepancy? Below, we show that this discrepancy is due, in large part, to the combined effect of the inability to resolve the individual monomers in the optical soot and the fractal nature of the clusters.

Resolution Correction. In our analysis, the number of primary particles present in the cluster is calculated from the cluster projected area using Eq. (2). This formula works well at high magnifications because the cluster and its monomers are well resolved. Problems arise, however, at low magnification because the individual monomers are not resolved. This problem does not lie in the relation $N \sim A^{\alpha}$, but in an erroneous determination of A due to the poor resolution. This, in turn, causes an error in N and hence k_0.

To understand this problem, consider the digitized image of a computer-generated DLCA cluster with fractal dimension 1.75 at two different magnifications in Fig. 2. The resolution limit is set by the pixel size. For example, the cluster at magnification 1 might yield $p_1 = 20$ nm/pixel, whereas magnification 2, twice that of magnification 1, might yield $p_2 = 10$ nm/pixel. The area (e.g., in nm^2) of the cluster is

$$A = np^2 \tag{14}$$

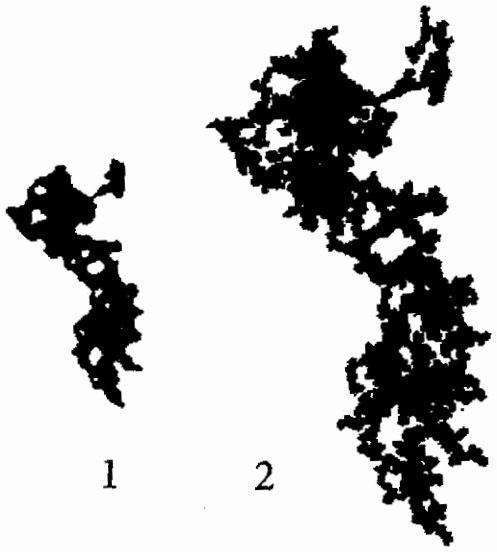

FIGURE 2. Computer-digitized image of a computer-generated DLCA cluster (D = 1.75) at two magnifications differing by a factor of two. At magnification two, additional structures are resolved.

where n is the number of pixels per cluster. If a higher magnification shows no new structure, then $A_1 = A_2$; hence,

$$n_2/n_1 = (p_1/p_2)^2. \tag{15}$$

That is, because the scale is larger by a factor of p_1/p_2, there are more pixels in the image of the cluster in 2 by a factor of $(p_1/p_2)^2$. The exponent 2 results because the dimension of the plane is two.

Now, consider the case where higher magnification reveals structure hidden at lower magnification as portrayed in Fig. 2. In this case, the fractal nature of the projection of the cluster implies that Eq. (15) should be modified to

$$n_2/n_1 = (p_1/p_2)^{D_2} \tag{16}$$

where, by Eq. (9), $D_2 = D_3/\alpha$ is the fractal dimension of the cluster when projected into the two-dimensional plane. From (14) and (16), we find

$$A_2/A_1 = (p_1/p_2)^{D_2-2}; \tag{17}$$

Aerosol Science and Technology
25:3 October 1996

then from Eqs. (1), (2), and (17), we find

$$k_{02}/k_{01} = (p_2/p_1)^{2\alpha - D} \quad (18)$$

where D is the fractal dimension of the cluster in three dimensions. Equation (18) can be used to compare k_0 values of the TEM and optical soot samples which were viewed at different magnifications. We remark that this correction can only be used between two regimes of unresolved monomers. Obviously, if the monomers are perfectly resolved at two different scales, Eq. (18) is invalid.

One might expect a correction due to resolution for R_g as well. We have been unable to calculate such a correction analytically. Simulations similar to Fig. 2 imply a random correction of a few percent for R_g. Given this uncertainty and randomness and the large correction necessary for N, we do not correct the R_g values.

The scales for our optical and TEM clusters are $p = 3500$ and 12.1 nm/pixel, respectively. Thus, using $\alpha = 1.09$ and $D = 1.78 \pm 0.05$, we find $k_0(\text{optical})/k_0(\text{TEM}) = 9.7 \pm 2.7$. Or using $\alpha = 1.042$ and $D = 1.70 \pm 0.05$, we find $k_0(\text{optical})/k_0(\text{TEM}) = 8.8 \pm 2.4$. When these corrections are applied to the two different analyses of the optical sample, the same "corrected" values of k_0, also given in Table 2, of 2.0 ± 0.9 are found. These values are consistent with the k_0 value obtained for the TEM sample. All of the data are plotted in Fig. 3. The large, $\sim 40\%$ error in the k_0 for the optical soot is due both to the fact that these data are far from the intercept (hence, a small uncertainty in slope acts as a lever arm on the plot, and k_0 is the intercept at $N = 1$), and the corrections of Eq. (18) have an exponential dependence on D so that the uncertainty in D is exponentially magnified. Because of these uncertainties, we consider

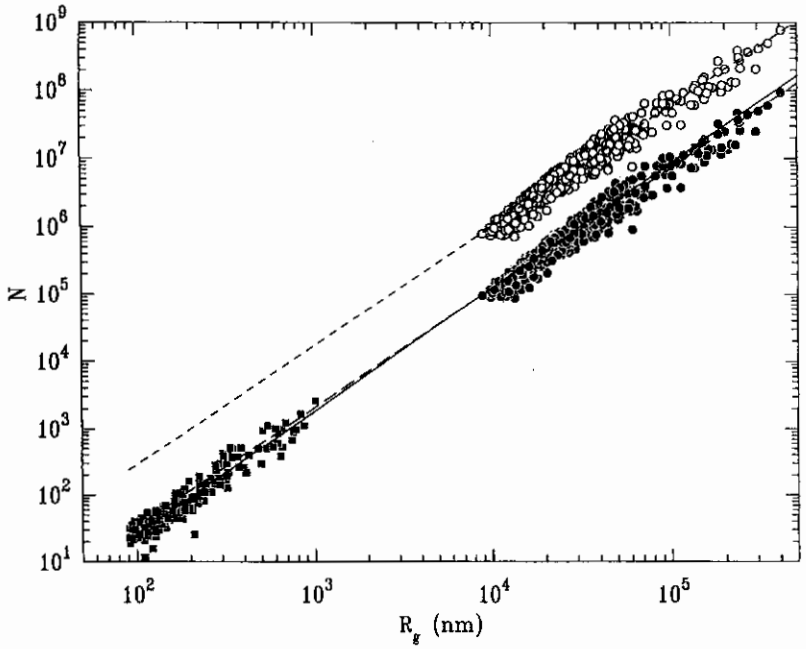

FIGURE 3. Number of monomers per cluster versus cluster radius of gyration for both thermophoretically sampled, TEM viewed soot (closed squares) and impaction sampled, optically viewed soot. For the latter, the open circles are uncorrected, the closed circles are corrected as described in the text. The lines are fits to Eq. (1) with D_f and k_0 given in Table 2.

the k_0 values for the optical sample to be only semi-quantitative.

CONCLUSIONS

Figure 3 demonstrates that the same morphology describes clusters ranging in size (R_g) from 50 nm to 400 μm, or in terms of N, the size ranges from 10 to 10^8, a seven order of magnitude range. This large range of constancy implies that the process by which the clusters are formed is the same over this vast size range. Since $D = 1.8$, it has been concluded that this process is Diffusion Limited Cluster Aggregation. The constancy of the morphology also implies that other physical properties of these clusters will be interrelated, and any variation would be due to comparisons of cluster length scales to lengths inherent in the given physical property.

This work was supported by a grant from NIST, 7ONANB4H1652, and a grant from the NSF Research Experiences for Undergraduates, PHY-9300250, and NSF Grant CTS-9408153. This work benefitted from discussions with Dr. G. W. Mulholland of NIST.

References

Bourrat, X., Oberlin, A., Van Damme, H., Gatean, C., and Bachela, R. (1988). *Carbon* 26:100–103.

Cai, J., Lu, N., and Sorensen, C. M. (1993). *Langmuir* 9:2861–2867.

Cai, J., Lu, N., and Sorensen, C. M. (1995). *J. Coll. Int. Sci.* 171:470–473.

Charalampopoulos, T. T., and Chang, H. (1991). *Combust. Flame* 87:89–99.

Dobbins, R. A., and Megaridis, C. M. (1987). *Langmuir* 3:254–259.

Forrest, S. R., and Witten, T. A. (1979). *J. Phys.* A12:L109–L117.

Gangopadhyay, S., Elminyawi, I., and Sorensen, C. M. (1991). *Appl. Opt.* 25:4859–4869.

Jullien, R., Thony, R., and Ehrburger-Doll, F. (1994). *Phys. Rev.* E50:3878–3882.

Koylu, U. O., and Faeth, G. M. (1992). *Combust. Flame* 89:140–156.

Koylu, U. O., and Faeth, G. M. (1994a). *J. Heat Transfer* 116:152–159.

Koylu, U. O., and Faeth, G. M. (1994b). *J. Heat Transfer* 116:971–979.

Koylu, U. O., Faeth, G. M., Farias, T. L., and Carvalho, M. G. (1995). *Combust. Flame* 100:621–633.

Meakin, P., Donn, B., and Mulholland, G. (1989). *Langmuir* 5:510–518.

Medalia, A. I., and Heckman, F. A. (1967). *J. Coll. Int. Sci.* 24:393–404.

Medalia, A. I., and Heckman, F. A. (1969). *Carbon* 7:567–582.

Megaridis, C. M., and Dobbins, R. A. (1990). *Combust. Sci. Technol.* 71:95–109.

Puri, R., Richardson, T. F., Santoro, R. J., and Dobbins, R. A. (1993). *Combust. Flame* 92:320–333.

Samson, R. J., Mulholland, G. W., and Gentry, J. W. (1987). *Langmuir* 3:272–281.

Sorensen, C. M., Cai, J., and Lu, N. (1992a). *Appl. Opt.* 31:6547–6557.

Sorensen, C. M., Cai, J., and Lu, N. (1992b). *Langmuir* 8:2064–2064.

Wu, M. K., and Friedlander, S. K. (1993). *J. Coll. Int. Sci.* 159:246–248.

Zhang, H. X., Sorensen, C. M., Ramer, E. R., Olivier, B. J., and Merklin, J. F. (1988). *Langmuir* 4:867–871.

Received December 5, 1995; revised March 1, 1996.